PEP: The star formation rates of 1.5<z<2.5 massive galaxies

R. Nordon[1], D. Lutz[1], L. Shao[1], B. Magnelli[1], S. Berta[1], B. Altieri[2], P. Andreani[3,11], H. Aussel[7], A. Bongiovanni[5,6], A. Cava[5,6], J. Cepa[5,6], A. Cimatti[8], E. Daddi[7], H. Dominguez[9], N.M. Förster Schreiber[1], R. Genzel[1], A. Grazian[10], G. Magdis[7], R. Maiolino[10], A.M. Pérez García[5,6], A. Poglitsch[1], P. Popesso[1], F. Pozzi[10], L. Riguccini[7], G. Rodighiero[4], A. Saintonge[1], M. Sanchez-Portal[2], P. Santini[10], E. Sturm[1], L. Tacconi[1], I. Valtchanov[2], M. Wetzstein[1], E. Wieprecht[1]

Introduction and data

The star formation rate (SFR) is a key parameter in the study of galaxy evolution. We are motivated to verify the accuracy of SFR measurements in z∼2 by a disagreement between previous observations and theoretical models. The latter predict SFRs that are typically a factor 4 lower than the measurements for this redshift. While UV and 24 μm luminosities were successful in measuring SFRs in large samples, UV-based SFRs are very sensitive to the extinction correction used and is the main cause of uncertainty. Estimates from the 24 μm luminosities rely on template-based extrapolations to the total IR luminosity that are poorly constrained at high z and may be affected by an AGN.

The photo-detector array camera and spectrometer (PACS) on-board Herschel observes at 160 μm, close to the peak of the emission from dust heated by young stars, away from AGN-heated dust emission and with un-precedented spatial resolution that reduces confusion noise.

We use PACS 160 μm data from *PACS Evolutionary Probe* (PEP) guaranteed-time observations in the GOODS-N field, to measure accurate SFRs for 1.5<z<2.5 galaxies and compare them to previous data.

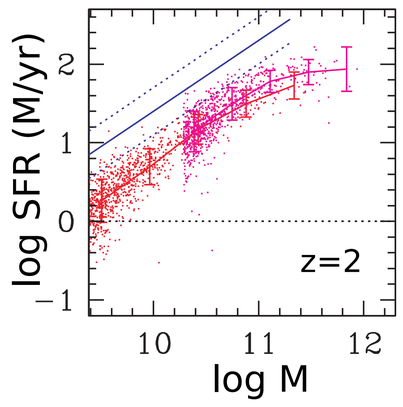

Figure 1: $M_\star$-SFR relation for simulations vs. observations. Red/magenta points with a running mean and stdev are from hydrosimulations. Solid blue lines indicate the mean of the UV-based SFRs from Daddi et al. (2007) with dotted lines indicating the spread. (Figure from Davé 2008)

FIR versus 24μm based SFR

SFRs based on 24 μm tend to over-estimate the true values by a mean factor ∼4 for LIRGS and increasing with luminosity to ∼7.5 for ULIRGS.

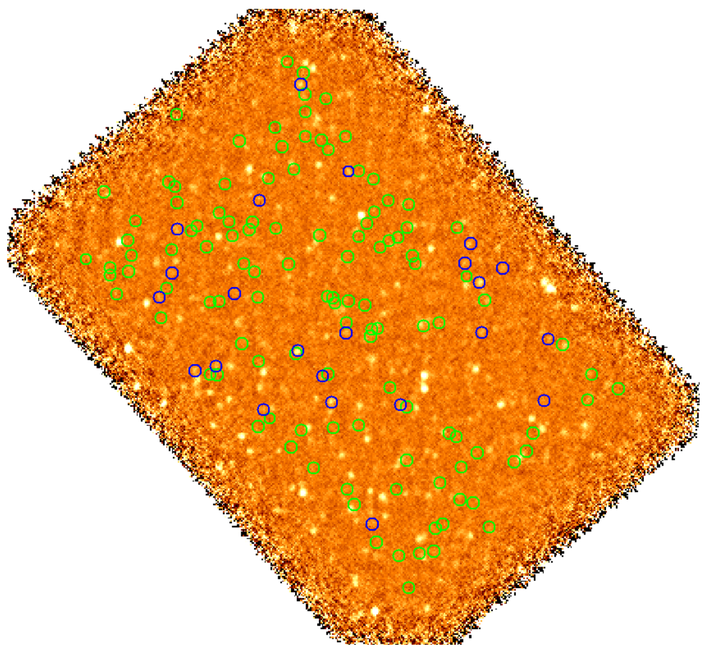

Figure 2: GOODS-N map in 160 μm with the positions of the 24 μm selected sample. PACS detected sources are in blue. Undetected sources, predicted to by ULIRGS by 24 μm, are in green. Undetected sources are stacked on a residual map from which all detected sources were removed.

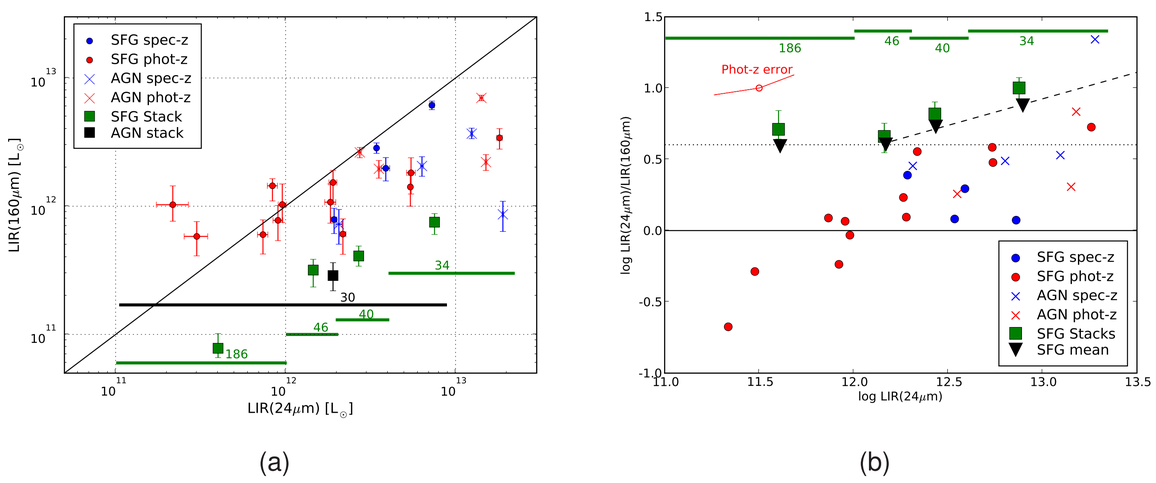

(a) (b)

Figure 3: **(a)** Total (8-1000 *mu*m) IR luminosity from 160 μm versus that derived from 24 μm. Detections with spec-z are in blue, detections with phot-z only are in red. SFGs are plotted as circles and AGNs as x marks. The error bars include only photometric errors. Squares represent mean luminosity of stacked SFG (green) and X-ray (**black**) undetected sources, with error bars indicating the error on the mean luminosity. Horizontal bars under the stacks indicate the min–max values in the stack with the number of stacked sources above them. **(b)** The log ratio of total IR luminosities (proportional to SFR) from 24 μm and 160 μm as a function of LIR from 24 μm. Colors and symbols are similar to (a) with **black** triangles representing the mean of all (detections and non-detections) SFGs in the stacked range. The red arrow at top left indicate the typical uncertainties due to phot-z errors. The dashed and dotted lines are ad-hoc fits that represent the general trend in the mean LIR(24 μm)/LIR(160 μm) ratio.

Spitzer-MIPS 24 μm fluxes are converted to LIR by fitting the 24 μm flux to CE01 SEDs. At z∼2 the rest-frame wavelengths are shorter than 10 μm and 24 μm fluxes probe the IR emission at the edge of the relevant range, far from the SED peak, making them sensitive to extrapolation errors. In addition, at these wavelengths polycyclic aromatic hydrocarbon (PAH) emission contribute significantly and the ratio between their fluxes and LIR may create significant scatter.

Fig. 3 shows that while there is some scatter, for most sources LIR(24 μm) is higher than LIR(160 μm). The detections appear to show a linear trend, however this is mostly due to a selection effect: The combined mean for the detection and non-detections (detected in stacks) is much higher and the individual detections represent a fraction of the distribution for which at a given LIR(24 μm), LIR(160 μm) is high enough to be detected.

X-ray AGNs do not seem to be different from the rest of the sample. The mean luminosity of the AGN stack is also similar to that of the SFG stacks. If the excess flux redshifted to 24 μm is due to hidden AGNs the nearly constant LIR(24 μm)/LIR(160 μm) ratio would imply a tight relation between the AGN luminosity and the galaxy's starburst component, which is not observed (Lutz et al. 2010, Shao et al. 2010). We conclude that while a hidden AGN may contribute to the scatter, it is not likely to be the main cause of the general 24 μm excess. Enhanced emission (relative to local galaxies SEDs) in PAH features that enter the 24 μm filter starting at z=1.5 is a more plausible explanation.

FIR versus UV based SFR

When using the Calzetti UV extinction law for SFR(UV)≳40 $M_\odot$ yr^{-1} galaxies, the SFRs tend to be overestimated by a mean factor ∼2 and with a scatter of a similar magnitude.

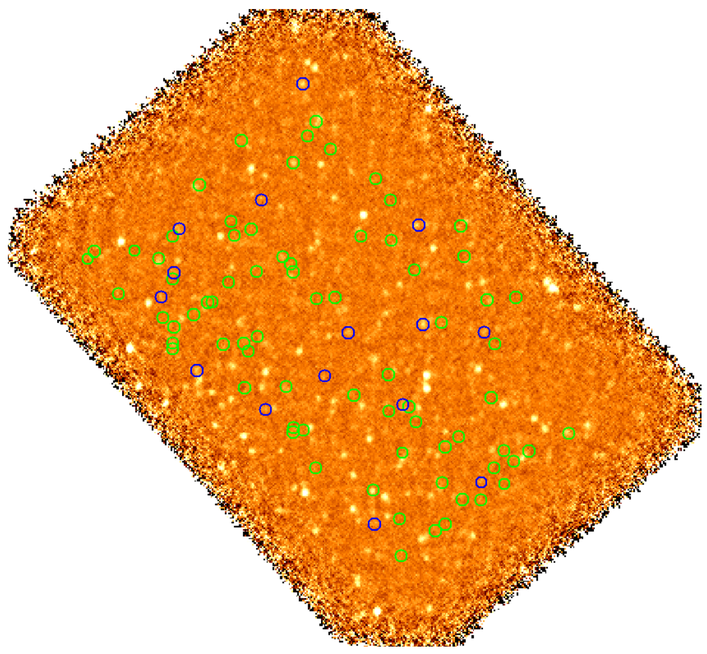

Figure 4: GOODS-N map in 160 μm with the positions of the BzK selected sample. PACS detected sources are in blue, undetected sources are in green. Undetected sources are stacked on a residual map from which all detected sources were removed.

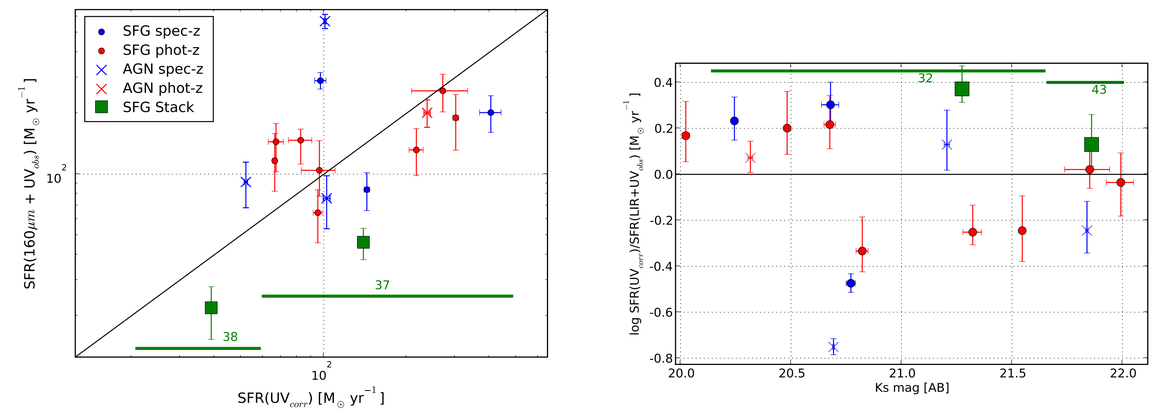

(a) (b)

Figure 5: **(a)** The sum of SFR from 160 μm and UV_{obs} (no attenuation correction) versus SFR derived from attenuation-corrected UV flux. Blue symbols are for spec-z, red are for phot-z. Circles are SFG detections, x-marks are AGNs. Errors on detected sources are photometric only. Green squares are mean SFR for stacks with the error on the mean. Horizontal bars below indicate the min–max range of values in the stack with the number of stacked sources noted above. **(b)** The log ratio of UV SFR over the combined LIR and UV_{obs} SFR versus Ks magnitude. Colors and symbols are the same as in (a)

We use B and z band photometry (probing rest frame ∼1500 Å and ∼3500 Å at z∼2) to estimate the SFR and dust attenuation. For the optical extinction we apply the calibration given by Daddi et al. (2004): $E(B-V) = 0.25(B-z+0.1)_{\rm AB}$ The effective attenuation at 1500 Å is obtained using the Calzetti et al. (2000) extinction law: $A_{1500} = 10E(B-V)$, which was derived for local starburst galaxies.

The Far infrared emission is assumed to be due to reprocessing of radiation from young stars by the dust and the addition of the SFR from the observed UV luminosity (Fig. 5) accounts for the escaped part of the UV radiation. The detections show a good agreement between $SFR(UV_{corr})$ and the combined $SFR(LIR+UV_{obs})$. When stacking the PACS non-detections, the $SFR(UV_{corr})$ for the stacks is slightly too high. The overall mean log-ratio of stacks and detections is 0.3 dex and the standard deviation is 0.35 dex.

References:

Calzetti, D., Armus, L., Bohlin, R. C. et al. 2000, ApJ, 533, 682
Chary, R. & Elbaz, D. 2001, ApJ, 556, 562
Daddi, E., Cimatti, A., Renzini, A. et al. 2004, ApJ, 617, 746
Daddi, E., Dickinson, M., Morrison, G. et al. 2007, ApJ, 670, 156
Davé, R. 2008, MNRAS, 385, 147
Elbaz, D., Hwang1, H.S., Magnelli, B. et al. 2010, A&A, Herschel special issue
Luts, D., Mainieri, V., Rafferty, D. et al. 2010, accepted to ApJ, arxiv 1002.0071
Shao, L., Luts, D., Nordon, R. et al. 2010, A&A Herschel special issue

Affilliations:

[1]MPI for Extraterrestrische Physik, Garching, Germany. [2]Herschel Science Centre. [3]ESO, Garching, Germany. [4]Department of Astronomy, University of Padova, Italy. [5]Instituto de Astrofísica de Canarias, Spain. [6]Departamento de Astrofísica, Universidad de La Laguna, Spain. [7]Laboratoire AIM, CEA/DSM-CNRS-Université Paris Diderot, IRFU/Service d'Astrophysique, France. [8]Dipartimento di Astronomia, Università di Bologna, Italy. [9]INAF - Osservatorio Astronomico di Bologna, Italy. [10]INAF - Osservatorio Astronomico di Roma, Italy. [11]INAF - Osservatorio Astronomico di Trieste, Italy.

nordon@mpe.mpg.de